Monthly Notices
of the
ROYAL ASTRONOMICAL SOCIETY
MNRAS **442,** 3737–3744 (2014) doi:10.1093/mnras/stu1127

Determination of mass and orbital parameters of a low-mass star HD 213597B

Priyanka Chaturvedi,[1]★ Rohit Deshpande,[2,3] Vaibhav Dixit,[1] Arpita Roy,[2,3] Abhijit Chakraborty,[1] Suvrath Mahadevan,[2,3] B. G. Anandarao,[1] Leslie Hebb[4] and P. Janardhan[1]

[1]*Astronomy and Astrophysics Division, Physical Research Laboratory, Ahmedabad 380009, India*
[2]*Department of Astronomy and Astrophysics, Pennsylvania State University, University Park, PA 16802, USA*
[3]*Center for Exoplanets and Habitable Worlds, The Pennsylvania State University, University Park, PA 16802, USA*
[4]*Department of Physics, Hobart and William Smith Colleges, Geneva, NY 14456, USA*

Accepted 2014 June 5. Received 2014 June 5; in original form 2013 December 31

ABSTRACT

HD 213597 is an eclipsing binary system which was detected by the *STEREO* spacecraft and was speculated to host a low-mass stellar companion. We used high-resolution spectroscopy with the 10-m Hobby–Eberly Telescope and the 1.2-m telescope in Mount Abu for radial velocity (RV) measurements of this source. We performed aperture photometry for this star on the *STEREO* archival data and thereby confirm the transit signature. We also did follow-up ground-based photometry with a 10-inch telescope from Mt Abu. The spectroscopic RV semi-amplitude of the primary (33.39 km s^{-1}) indicates that the secondary is an M dwarf making the system a short period F+M eclipsing binary. These RVs along with the inclination derived from our combined photometric analysis ($i = 84.^{\circ}9$), enable us to estimate the mass of the secondary as $M_B \sim 0.286\,M_{\odot}$ and radius as $R_B \sim 0.344\,R_{\odot}$ using an estimated mass $M_A \sim 1.3\,M_{\odot}$ and radius $R_B \sim 1.97\,R_{\odot}$ of the primary. Our spectral analysis returned the following parameters: $T_{\rm eff} = 6625 \pm 121$ K, [Fe/H] $= -0.095 \pm 0.08$ and $\log g = 3.72 \pm 0.22$ for the primary. When $\log g$ is constrained to a value of 3.96, we derive $T_{\rm eff} = 6753 \pm 52$ K and [Fe/H] $= -0.025 \pm 0.05$.

Key words: techniques: photometric – techniques: radial velocities – binaries: eclipsing – stars: individual: HD 213597 – stars: low-mass.

1 INTRODUCTION

Mass and radius are the two fundamental properties of a star that allow us to determine their age, evolution and luminosity (Andersen 1991). Through careful photometry and spectroscopy of detached single- and double-lined eclipsing binaries, it is possible to obtain radii and masses of individual components to as high accuracies as 1 per cent for double-lined eclipsing binaries. Such precise measurements impose strong constraints on stellar evolution models. In recent years, such measurements have revealed discrepancies between observed and model-derived stellar radii of low-mass stars (Torres, Andersen & Giménez 2010). For stars with masses below $0.5\,M_{\odot}$, the measured radii appear to be 20–30 per cent larger than predicted (López-Morales 2007). One hypothesis suggests that this disagreement is caused by the degree of magnetic activity in stars: strong magnetic fields inhibit convection causing stars to inflate their radii (Mullan & MacDonald 2001; López-Morales & Ribas 2005). Another hypothesis suggests metallicity dependency on radii inflation: Berger et al. (2006) in their study find that the disagreement is larger among metal-rich stars than metal-poor stars. They conclude that current atmospheric models do not take into account opacity sources which may lead to such discrepancy. Therefore, it becomes imperative to discover more such systems and determine their masses and radii to very high precision.

F-type stars are typically fast rotators with a tenuous convective zone. Bouchy et al. (2011a) suggest that there is a higher probability of M dwarfs orbiting F-type primaries, in contrast to G-type primaries. Bouchy et al. (2011a,b) further suggest that for a massive companion to exist around a primary star, the total angular momentum must be above a critical value. If a primary star has a smaller spin period than the orbital period of the system (as in the case for G-type stars), the tidal interactions between the two stars will cause the secondary companion to be eventually engulfed by the primary. However, this is less likely to occur among fast rotating F-type stars which have weaker magnetic braking and can avoid the spin-down caused due to the tides raised by the massive secondary. This helps the companions around F-type stars to survive rapid

★ E-mail: priyanka@prl.res.in

Table 1. Stellar properties of host star HD 213597A from literature.

Parameter	Value	Reference
Mass	1.5 ± 0.1 M$_\odot$	(1)
Radius	2.039 ± 0.303 R$_\odot$	(2)
log g	3.99 ± 0.05	(1)
$v \sin i$	40 ± 5 km s^{-1}	(3)
$T_{\rm eff}$	6837 ± 80 K	(1)
[Fe/H]	-0.14 ± 0.1	(1)
Age	1.90 ± 0.2 Gyr	(1)
Distance	115 ± 15 pc	(4)
V magnitude	7.8	(5)
RA (epoch=2000)	$22^{\rm h}32^{\rm m}32\overset{\rm s}{.}626$	(5)
Dec. (epoch=2000)	$1^\circ 34' 56\overset{''}{.}83$	(5)

References: (1) Casagrande et al. (2011); (2) Masana et al. (2006); (3) Nordström et al. (2004); (4) from *Hipparcos* data; (5) from SIMBAD.

orbital decay due to loss of angular momentum. F-type primaries with M-type secondaries (hereafter F+M binaries) are often discovered in transit surveys, which are primarily designed to search for transiting planets (e.g. Bouchy et al. 2005; Beatty et al. 2007). Over the last few years a handful of F+M binaries have been discovered and their properties determined (e.g. Pont et al. 2005a,b, 2006; Fernandez et al. 2009). Nonetheless, every additional system discovered and analysed contributes more to our understanding of fundamental stellar properties making the sample of F+M binaries an important subset of stellar studies.

The NASA *STEREO* mission consists of two satellites in the heliocentric orbit that study the Sun and its environment. An imager on one of the satellites is being employed to study the variability of bright stars and to look for transiting exoplanets. Observations taken by the *STEREO* spacecraft were analysed by Wraight et al. (2012) to search for low-mass eclipsing companions to bright stars with effective temperatures between 4000 and 7000 K and visual magnitude $6 < V < 12$. The *STEREO* Heliospheric Imagers (HIs) have a field of view of $20^\circ \times 20^\circ$ and a 2048×2048 element CCD with a spectral response that peaks between 6300 and 7300 Å (Wraight et al. 2012). HD 213597 was one of the nine candidates selected (Wraight et al. 2012) where the radius of the secondary was estimated to be below 0.4 R$_\odot$. HD 213597A, with a visual magnitude of 7.8, is an F-type star having a rotational velocity of 40 km s^{-1} (Nordström et al. 2004) and a radius of 2.039 R$_\odot$ (Masana, Jordi & Ribas 2006). Table 1 lists the properties of this star obtained from the literature. The earlier studies on this star suggest that it may host a low-mass companion.

Here, we describe high-resolution spectroscopic and photometric observations and the methods of analysis used to derive the physical parameters concerning HD 213597 system. Details of the spectroscopic observations and transit photometry are reported in Section 2, while Section 3 describes the analytic methods and main results. Discussion and conclusions are presented in Section 4.

2 SPECTROSCOPIC AND PHOTOMETRIC OBSERVATIONS OF HD 213597

2.1 Spectroscopy

High-resolution spectroscopic observations of the star HD 213597A were made with the fibre-fed high-resolution spectrograph (HRS; Tull 1998) at the 10-m McDonald Hobby–Eberly Telescope (HET; Ramsey et al. 1998), and the fibre-fed echelle spectrograph, Physical Research Laboratory Advanced Radial Velocity Abu-sky Search (PARAS; Chakraborty et al. 2014) at the 1.2-m telescope at Gurushikhar Observatory, Mount Abu, India.

2.1.1 *HET-HRS observations*

We obtained nine observations between 2011 October and 2012 July using the HRS in its 316g5936 cross-disperser setting, 2 arcsec diameter fibre, resolution of ∼30 000 and a simultaneous wavelength coverage of 4300–5800 and 6200–7600 Å. The exposure times ranged between 60 and 300 s, which yielded signal-to-noise ratio (S/N) between 200 and 600 per resolution element. Each observation was bracketed before and after with a thorium–argon (ThAr) lamp exposure for wavelength calibration. The same procedure was used on HD 215648, which served as a template to derive radial velocities (RVs). HD 215648 has a spectral type of F7V with $T_{\rm eff} = 6228 \pm 100$ K, $\log g = 4.15 \pm 0.07$ (Edvardsson et al. 1993), $v \sin i = 6.7 \pm 0.7$ km s^{-1} (Ammler-von Eiff & Reiners 2012) and [Fe/H] $= -0.22$ (Valenti & Fischer 2005). The data were reduced using a custom optimal extraction pipeline as described in Bender et al. (2012).

2.1.2 *Mt Abu-PARAS observations*

A total of 15 observations were taken between October and November 2012 using the fibre-fed PARAS spectrograph which has a single prism as a cross-disperser, a blaze angle of 75° and a resolution of 67 000. The exposure time for each observation was fixed at 1200 s which resulted in S/N between 20 and 25 pixel^{-1} at the blaze wavelength. Simultaneous exposures of the science target and the ThAr lamp for wavelength calibration were taken. The wavelength region between 3700 and 6800 Å was considered for the RV measurements. The data were reduced by the Interactive Data Language (IDL) pipeline designed specifically for PARAS as described in Chakraborty et al. (2014).

2.1.3 *Errors on radial velocity measurements*

The precision on RV measurements (Hatzes & Cochran 1992) is given as $\sigma \sim 1.45 \times 10^9 ({\rm S/N})^{-1} R^{-1} B^{-1/2}$ m s^{-1}, where S/N is the signal-to-noise ratio of the spectra, while R and B are the resolving power and wavelength coverage of the spectrograph in angstrom (Å), respectively. Although PARAS has much higher resolution than the HET-HRS mode that was used, the S/N of PARAS spectra is lower, leading to the PARAS RVs having larger uncertainties than the HET-HRS RVs. As mentioned earlier, HD 213597A is an early F-type star with a rotational velocity of 40 km s^{-1}. Bouchy, Pepe & Queloz (2001) defined a quality factor Q that represents the quality and spectral line richness of the spectrum. It was further shown that Q deteriorates with increasing rotational velocity thereby increasing the RV uncertainty. For instance, a F2-type star with a rotational velocity of 40 km s^{-1} has a RV uncertainty 10 times larger than one that is rotating at 4 km s^{-1}. The covariant errors obtained from fitting the peak of the cross-correlation function in IDL are reported as uncertainties on the HET data. For PARAS spectra, errors based on photon noise are computed for each spectrum as discussed in Bouchy et al. (2001). Since HD 213597A has a RV semi-amplitude of ∼33 km s^{-1}, for a relatively small orbital period of 2.4238 d, the RVs get smeared within the duration of the exposure as a function of orbital phase. The orbital smearing errors were estimated and

Table 2. Observations for the star HD 213597. The time in UT and BJD–TDB are mentioned in first two columns followed by exposure time and barycentric corrected RV in third and fourth column, respectively. The next two columns have RV errors, fifth column corresponds to covariant errors (HET-HRS) or photon noise errors (PARAS) and column 6 has orbital smearing errors. Last column is the instrument used for observations.

UT date	T-240 0000 (BJD–TDB)	Exp. time (s)	RV (km s^{-1})	σ-RV (km s^{-1})	σ-orbital smearing (km s^{-1})	Instrument (flag)
2011 Oct 30	55864.689	250	4.844	0.209	0.167	HET-HRS
2011 Nov 25	55890.614	60	11.822	0.208	0.030	HET-HRS
2011 Nov 27	55892.609	180	−20.967	0.214	0.116	HET-HRS
2011 Dec 15	55910.552	60	15.026	0.212	0.026	HET-HRS
2012 Jun 11	56089.949	300	14.561	0.210	0.142	HET-HRS
2012 Jun 22	56100.924	300	−30.586	0.217	0.162	HET-HRS
2012 Jun 23	56101.918	300	19.909	0.212	0.064	HET-HRS
2012 Jul 01	56109.905	180	−27.993	0.204	0.103	HET-HRS
2012 Jul 02	56110.901	300	−9.125	0.214	0.203	HET-HRS
2012 Oct 17	56218.260	1200	2.940	0.148	0.255	PARAS
2012 Oct 17	56218.276	1200	2.905	0.176	0.290	PARAS
2012 Oct 17	56218.292	1200	2.134	0.180	0.325	PARAS
2012 Oct 18	56219.210	1200	−61.491	0.248	0.253	PARAS
2012 Oct 18	56219.225	1200	−61.522	0.242	0.219	PARAS
2012 Oct 18	56219.241	1200	−62.592	0.226	0.185	PARAS
2012 Oct 21[a]	56222.269	1200	−42.356	0.267	0.805	PARAS
2012 Oct 21[a]	56222.285	1200	−36.462	0.283	0.813	PARAS
2012 Oct 23	56224.198	1200	−62.984	0.148	0.051	PARAS
2012 Oct 23	56224.214	1200	−62.904	0.158	0.085	PARAS
2012 Nov 7	56239.202	1200	−42.605	0.148	0.763	PARAS
2012 Nov 7	56239.219	1200	−40.721	0.155	0.773	PARAS
2012 Nov 7	56239.234	1200	−39.516	0.167	0.783	PARAS
2012 Nov 8	56240.179	1200	0.438	0.188	0.479	PARAS
2012 Nov 8	56240.195	1200	−1.008	0.183	0.511	PARAS

[a]Not considered for RV analysis.

added quadratically with the photon noise and covariant errors for both PARAS and HET data points and used as uncertainties for individual RV points. The barycentric corrected RV values along with the associated uncertainties are mentioned in Table 2. Over the course of 1 yr (2011 October–2012 November) we obtained a combined total of 24 observations with the two spectrographs. Two epochs from the observed RVs of PARAS data were removed in the fitting routine because of very low S/N (due to passing clouds).

2.2 Transit photometry

We performed ground-based photometric observations for this star from the calculated mid-eclipse time based on the ephemeris of Wraight et al. (2012). Given the celestial coordinates of the star (refer Table 1) and the prolonged monsoon in India, we get a narrow window of 3 weeks in the month of October to observe the complete transit of the object. Thus, we also revisited the archival *STEREO* data (Wraight et al. 2012), in order to compute the transit parameters like transit duration and angle of inclination in combination with our ground-based photometry at Physical Research Laboratory (PRL), Mount Abu, India.

STEREO data from HI-1A instrument were extracted from the UK Solar System Data Centre (UKSSDC) website.[1] The star was observable for a period of 16–17 d on the CCD for each cycle of observation. Six such cycles of data were used for HD 213597A between the period 2008 January to 2012 October. For our purposes, we used L2 images, which were pre-processed (bias subtracted and flat-fielded) and accounted for solar coronal contamination. The wavelength band of observation is narrowly peaked between 630 and 730 nm (Wraight et al. 2012). A total of 36 transits for HD 213597A were recorded in six cycles of the extracted data.

We also obtained follow-up photometric observations of HD 213597A with the PRL 10-inch telescope at Gurushikhar, Mount Abu, India. We carried out photometry on 2013 October 21 UT for a duration of 5 h. The observations were carried out using a Johnson *R* band with a back thinned E2V 1k × 1k CCD array with a field of view of 46 × 46 arcmin^2. A mismatch of the dome position while guiding resulted in the rejection of an hour-long observation. Furthermore, due to passing clouds, we lost about 20 per cent of the egress time. Despite the data loss, we detected the transit at a confidence level of 4σ.

3 ANALYSIS AND RESULTS

3.1 Radial velocity measurements

3.1.1 HET-HRS

The reduced data were wavelength calibrated and continuum normalized while the echelle orders were stitched to produce a continuous 1D spectrum between two wavelength regions of 4300–5800 and 6200–7500 Å. The spectrum was then divided into eight segments (4386–4486, 4593–4843, 4925–5025, 5100–5410, 5475–5800, 6365–6430, 6620–6850, 7450–7500 Å) that are free of telluric lines. Each segment was cross-correlated using a 1D cross-correlation algorithm. The resulting 1D correlation arrays were

[1] www.ukssdc.rl.ac.uk

Table 3. Spectroscopically determined stellar parameters of HD 213597A (this work). The two measurements listed for each stellar parameter results from two SME run: (1) when all parameters are allowed to float; (2) when $\log g$ is fixed to a value determined by mass and radius measurements.

Stellar parameter	Value (free parameters)	Uncertainty	Value (constrained fitting)	Uncertainty
$T_{\rm eff}$ (K)	6625	±121	6752	±52
$\log g$	3.72	±0.22	3.96	–
[Fe/H]	−0.095	±0.08	−0.025	±0.05
[M/H]	−0.156	±0.03	−0.105	±0.03
$v\sin i$ (km s^{-1})	39.53	±1.3	39.53	±1.3
Microturbulence (km s^{-1})	2	–	2	–

combined using the maximum likelihood method (Zucker 2003). We employed a robust non-linear least-square curve fitting algorithm, MPFIT in IDL, to fit the peak of the cross-correlation function and determine the RVs and the associated errors.

3.1.2 Mt Abu-PARAS

The entire reduction and analysis for PARAS was carried out by the custom-designed pipeline in IDL based on the REDUCE optimal extraction routines of Piskunov & Valenti (2002). The pipeline performs the routine tasks of cosmic ray correction, dark subtraction, order tracing and order extraction. A complete thorium line list for the PARAS spectral range is utilized. The wavelength calibration algorithms were specifically optimized for PARAS as described in Chakraborty et al. (2014). The RV values were computed by cross-correlating the observed spectra against an F-type binary mask. Barycentric corrections were applied to all the RV points by standard IDL routines. The binary mask was created with the SPECTRUM program (Gray 2009) using Kurucz stellar atmosphere models with a temperature of $T_{\rm eff} = 6750$ K, $\log g = 4.0$ and a metallicity [M/H] = −0.2 (refer Table 1).

3.2 Spectral analysis

We based our spectral analysis of HD 213597A on the SME (Valenti & Piskunov 1996) spectral synthesis code. SME is composed of a radiative transfer engine that generates synthetic spectra from a given set of trial stellar parameters and a Levenberg–Marquardt solver that finds the set of parameters (and corresponding synthetic spectrum) that best matches observed input data in specific regions of the spectrum. The basic parameters that we used to define a synthetic spectrum are effective temperature ($T_{\rm eff}$), surface gravity ($\log g$), metallicity ([M/H]), iron abundance relative to solar ([Fe/H]) and projected rotational velocity ($v\sin i$). In order to match an observed spectrum, we solved for these five parameters. SME was implemented by using the Advanced Computing Centre for Research and Education (ACCRE) High-Performance Computing Center at Vanderbilt University for a large number (150) of different initial conditions to fully explore the χ^2 space and find the optimal solution at the global minimum. In addition, we applied a line list based on Stempels et al. (2007) that is suited for hotter stars, used the MARCS model atmosphere grid in the radiative transfer engine, and obtained the microturbulence ($v_{\rm t}$) from the polynomial relation defined in Gómez et al. (2013).

We applied our SME pipeline to the high S/N HET spectrum of HD 213597A allowing all five parameters listed above to vary freely. We obtained $T_{\rm eff} = 6625 \pm 121$ K, $\log g = 3.72 \pm 0.22$ and [Fe/H] $= -0.095 \pm 0.08$. It is important to note that for hotter stars, uncertainties on the gravity derived from spectral synthesis increase because the wings of the Mg I b triplet at 5167, 5172 and 5183 Å used to constrain this parameter become narrower and less sensitive to gravity. We also ran our SME pipeline again, this time constraining $\log g = 3.96 \pm 0.1$ based on the literature cited value. In this set of 150 trials, we fixed the gravity to a randomly chosen value within this range and solve for the other four parameters. For the constrained run, we obtained $T_{\rm eff} = 6752 \pm 52$ K, iron abundance ([Fe/H]) $= -0.025 \pm 0.05$ and metallicity ([M/H]) $= -0.105 \pm 0.03$.

The formal 1σ errors are based on the $\delta\chi^2$ statistics for the five free parameters. To derive the systematic uncertainties, we compared the results of our pipeline to three independent data sets with parameters in the literature (Valenti & Fischer 2005; Torres et al. 2012; Huber et al. 2013) and report the mean absolute deviation of our results compared to all the comparison stars. The final results (both free and constrained $\log g$) are listed in Table 3 along with their combined statistical and systematic uncertainties. Fig. 1 shows a sample of the observed spectrum (solid line) overlaid by the best-fitting model obtained by a free parameter fit ($T_{\rm eff} = 6625$ K, [Fe/H] $= -0.095$, $\log g = 3.72$, dotted line). The observed and model spectra are shown across the wavelength region 5160–5190 Å, including the Mg I b triplet.

3.3 Transit

The *STEREO* images from HI, HI-1A, L2 data are a priori bias and flat corrected. These files have a field of view of 20° × 20° imaged on a 2k × 2k CCD. The data were 2 × 2 binned on a 1k × 1k image with a field of view of 70 × 70 arcsec^2 pixel^{-1}. Each image is a sum of 30 exposures with a total exposure time of 20 min and an observational cadence of 40 min (Wraight et al. 2011). The procedure given in Sangaralingam & Steven (2011) was followed to do aperture photometry on the data. An aperture of 3.5 pixels was chosen for the same. We used the standard IRAF[2] DAOPHOT package for processing the photometry data. The flux computed by IRAF was detrended by fitting a fourth-order polynomial to account for the CCD response function as discussed in Sangaralingam & Steven (2011). The data were further normalized for each cycle. The rms scatter on the light curve for the source star outside the transit time duration is 7 mmag. A total of 36 transits were obtained for the entire data of six cycles between the period 2008 January–2012 October.

For the ground-based photometry observations from Mt Abu on 2013 October 21, each individual frame had an exposure time of 2 s and a readout time of ∼1 s. Similar to the *STEREO* data, IRAF

[2] IRAF is distributed by the National Optical Astronomy Observatory, which is operated by the Association of Universities for Research in Astronomy, Inc., under cooperative agreement with the National Science Foundation.

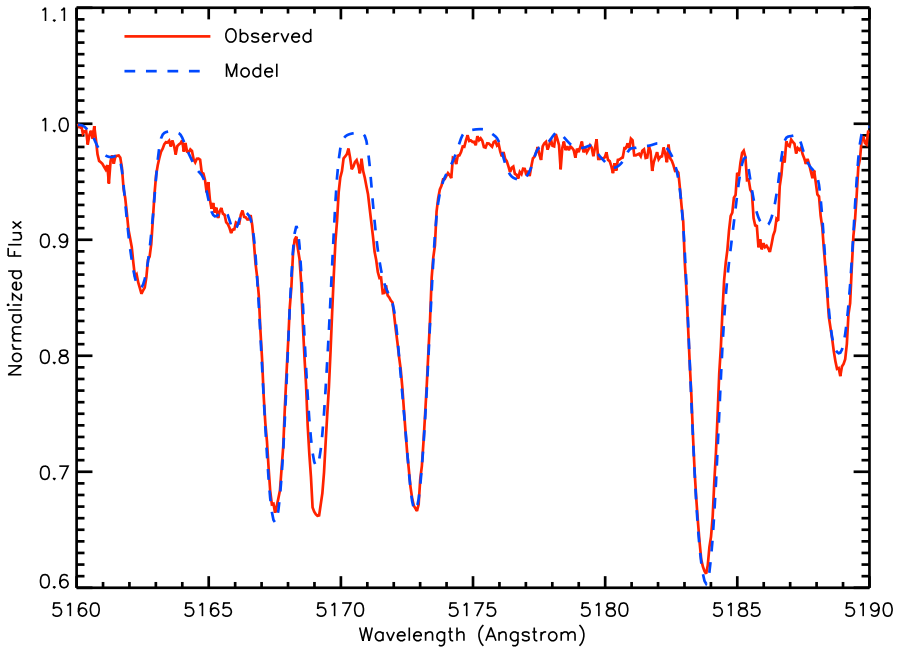

Figure 1. Observed normalized spectra (solid line) plotted across the wavelength region of 5160–5190 Å covering the Mg I triplet at 5167, 5172 and 5183 Å. Overplotted is the modelled spectra (dash line) obtained from SME analysis (when all parameters are kept free), with temperature value of $T_{\rm eff}$ of 6625 K, [Fe/H] of 0.095 and log g of 3.72.

DAOPHOT package was used to perform aperture photometry on the data. The frames were flat-fielded and dark corrected. Varying airmass and other local sky variations are accounted for, to an extent, by performing differential photometry on a comparison star and a check star. For differential photometry, we need a comparison star which is non-varying with time and is similar in colour and magnitude to the program star. We chose HD 213763 with spectral type F5V and a visual magnitude of 7.8 as the comparison star. In order to cross-check the non-variability of the comparison star, we required another field star called check star, which in our case was HD 213598 (K0V with a visual magnitude of 9.14). Although it is desirable to choose a check star of similar colour as that of the source and comparison stars, we settled for a K-type check star due to unavailability of bright field stars in the near vicinity. Since we used the Johnson *R* band for our photometry observations, the effect of scattering by moonlight and the atmospheric extinction was minimal. The average S/N of the source and the comparison star was between 300 and 350 for individual frames. 60 consecutive frames of similar exposures were median combined to avoid the scintillation noise from sky which, otherwise, becomes the dominant source of noise. Thus, each binned data frame comprised a total exposure time of 120 s and a total time cadence of 202 s (including the readout time) making the S/N of the combined frame to be ∼2500 for the same stars. Differential photometry was performed on the program star, HD 213597A and additional two bright field stars (HD 213763 and HD 213598). Individual light curve of comparison and check star showed a rms scatter of 12 mmag over the entire observation period. The rms scatter between the comparison and the check star reduced to 6 mmag after differential photometry. This formed the base level for detection of any transit and thus reflected the photometric error on each data point in the light curve. The data from *STEREO* and PRL 10-inch telescope were combined to produce a phase-folded light curve as both the data sets were observed in *R* band and had similar photometric errors on them.

3.4 Simultaneous spectroscopy and photometry fitting

We simultaneously fit the spectroscopy and photometry data with EXOFAST (Eastman, Gaudi & Agol 2013). EXOFAST is a set of IDL routines designed to fit transit and RV variations simultaneously or separately, and characterize the parameter uncertainties and covariances with a Differential Evolution Markov chain Monte Carlo method (Johnson et al. 2011). It can either fit RV and transit values exclusively or use both data sets to give a simultaneous fit. It also requires priors on $T_{\rm eff}$, log g and iron abundance [Fe/H]. EXOFAST uses empirical polynomial relations between masses and radii of stars; their log g, $T_{\rm eff}$ and [Fe/H] based on a large sample of non-interacting binary stars in which all of these parameters were well measured (Torres et al. 2010). These priors are used as a convenient way of modelling isochrones and are fast enough to incorporate them at each step in Markov chain. The errors derived here are determined by evaluating the posterior probability density based on the range of a given parameter that encompasses some set fraction of the probability density for the given model. We thereby caution the reader that the errors reported here for the mass and radius of the secondary are formal errors from EXOFAST. These values and errors are themselves based on models and isochrones and should not be used as independent observational checks on these models until more precise values can be derived in the future by teasing out a double-lined spectroscopy orbital solution for this system.

We executed the EXOFAST routine with the combined RV data sets (HET-HRS and PARAS) and the combined photometry data sets (one from the transit light curve obtained by *STEREO* and the other one obtained by PRL 10-inch telescope). On varying the SME-derived parameters as input priors to EXOFAST, we found that constraining log g with the same uncertainties as given in Table 3 yielded the most consistent values for $T_{\rm eff}$ and [Fe/H] (best simultaneous fit for RV and transit data). The results of the execution are summarized in Table 4. Fig. 2 illustrates the RV versus orbital

Table 4. Results obtained from EXOFAST by simultaneous fitting of RV and transit data for HD 213597 with a 68 per cent confidence interval.

Parameter	Units	Values
HD 213597A		
M_A	Mass ($M_\odot$)	$1.293^{+0.12}_{-0.1}$
R_A	Radius ($R_\odot$)	$1.973^{+0.085}_{-0.080}$
L_A	Luminosity ($L_\odot$)	$7.04^{+0.60}_{-0.52}$
ρ_A	Density (cgs)	$0.2377^{+0.0054}_{-0.0053}$
$\log g_A$	Surface gravity (cgs)	3.96 ± 0.01
$T_{\rm eff}$	Effective temperature (K)	6699^{+53}_{-52}
[Fe/H]	Iron abundance	$-0.065^{+0.050}_{-0.048}$
HD 213597B		
e	Eccentricity	$0.0198^{+0.0094}_{-0.0091}$
ω_*	Argument of periastron (°)	72^{+12}_{-18}
P	Period (d)	$2.4238503^{+0.000017}_{-0.0000019}$
a	Semimajor axis (au)	$0.04112^{+0.00058}_{-0.00057}$
M_B	Mass ($M_\odot$)	$0.286^{+0.012}_{-0.01}$
R_B	Radius ($R_\odot$)	$0.344^{+0.0097}_{-0.01}$
ρ_B	Density (cgs)	$9.32^{+0.43}_{-0.41}$
$\log g_B$	Surface gravity	$4.803^{+0.0093}_{-0.0097}$
RV parameters		
$e\cos\omega_*$		$0.0056^{+0.0043}_{-0.0042}$
$e\sin\omega_*$		$0.0184^{+0.0096}_{-0.0097}$
$T_{\rm P}$	Time of periastron (BJD)	$245\,5392.09^{+0.087}_{-0.12}$
K	RV semi-amplitude m s^{-1}	33390^{+290}_{-280}
M_B/M_A	Mass ratio	0.2218 ± 0.0045
γ	Systemic RV m s^{-1}	-4420^{+180}_{-190}
$f(m)$	Mass function[a] ($M_\odot$)	0.0091 ± 0.000048
Transit parameters		
$T_{\rm C}$	Time of transit (BJD)	$245\,5392.2014^{+0.0015}_{-0.0016}$
R_B/R_A	Radius of secondary in terms of primary radius	0.178 ± 0.001
i	Inclination (°)	$84.9^{+0.61}_{-0.50}$
a/R_A	Semimajor axis in stellar radii	$4.48^{+0.039}_{-0.038}$
δ	Transit depth	$0.0317^{+0.0013}_{-0.0012}$
T_{14}	Total transit duration (min)	274^{+5}_{-4}

[a]By BOOTTRAN (IDL).

phase for HD 213597A. Solid and open circles (top panel) show RV measurements of the primary taken with the HRS and PARAS instruments, respectively. The figure also shows the residuals (observed model) in the bottom panel. There are four RV measurements for this star from Nordström et al. (1997) observed with the 1.5-m Wyeth reflector at the Oak Ridge Observatory in Harvard, MA. We corrected for the offset in RV and overplotted these points in Fig. 2 to give it a longer time base. However, we did not include these points in the model due to their relatively large errors. It is important to note that despite a long time-gap between our observations and those of Nordström et al. (1997), their RV measurements (asterisks) lie on the model curve as shown in Fig. 2.

Fig. 3 (upper panel) shows the simultaneous fit for the transit light curve obtained by analysing *STEREO* archival data (filled circles) and PRL 10-inch telescope data (open squares) overplotted with the model derived from EXOFAST (solid curve). The residuals are plotted in lower panel. The simultaneous fit gives us a transit depth of $0.0317^{+0.0013}_{-0.0012}$ mag, angle of inclination of $84.^{\circ}9^{+0.62}_{-0.5}$ and a transit time duration of 274^{+5}_{-4} min. The transit depth cited here is consistent with the refined analysis of *STEREO* light curve by Whittaker, Stevens & Sangaralingam (2013). We obtain the mass of the secondary as $0.286^{+0.012}_{-0.01}$ $M_\odot$ and a radius of $0.344^{+0.0097}_{-0.01}$ $R_\odot$. We also calculated the mass function for this system by using the IDL BOOTTRAN package (Wang et al. 2012). The results obtained by the combined RV and transit data sets are consistent with the period 2.4238 d (Wraight et al. 2012; Whittaker et al. 2013) with a semimajor axis of 4.48 $R_\star$ (0.041 au) and a RV semi-amplitude of 33.39 km s^{-1}. Based on the mass limits, we conclude that the secondary star is an early M dwarf (Baraffe & Chabrier 1996).

4 DISCUSSION AND CONCLUSIONS

Using high-resolution spectroscopy taken with the HET-HRS, PARAS spectrographs and photometry with the *STEREO* data, PRL 10-inch telescope, we conclude that HD 213597 is an eclipsing binary system with an F-type primary and an early M-type secondary. The estimated secondary mass from RV measurements is $M_B = 0.286^{+0.012}_{-0.01}$ $M_\odot$ with an accuracy of ∼3–4 per cent (formal

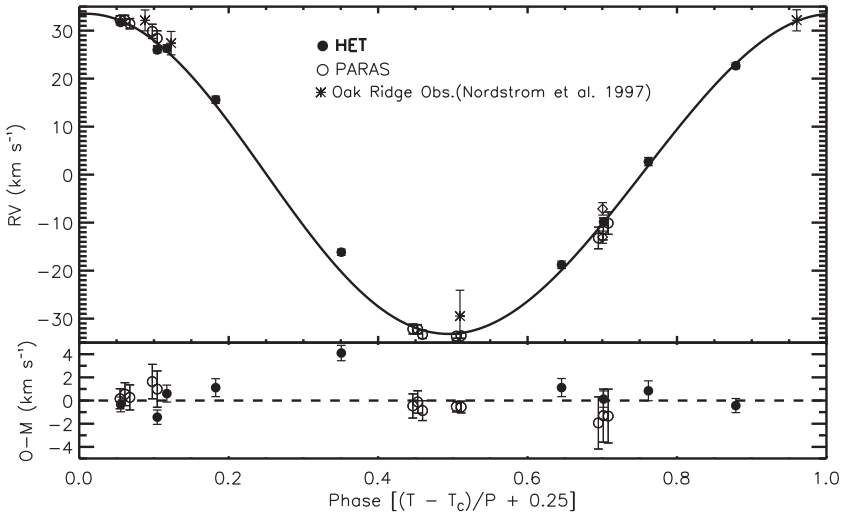

Figure 2. Top panel: RV model curve for star HD 213597 obtained from EXOFAST is plotted against orbital phase. HRS-HET (filled circles) and PARAS, Mount Abu (open circles) observed data points along with the estimated errors are overplotted on the curve. The two data points from PARAS not considered for RV fitting are overplotted with diamonds. The four RV measurements (not considered for RV fitting) from Nordström et al. (1997) are overplotted on the modelled data. Bottom panel: the residuals from best-fit are plotted below the RV plot. The residuals are not plotted for the points which are not considered for the RV fitting. For better visual representation, the *x*-axis in phase is shifted by 0.25 so that the central primary transit crossing point (T_c) occurs at phase 0.25 instead of 0.

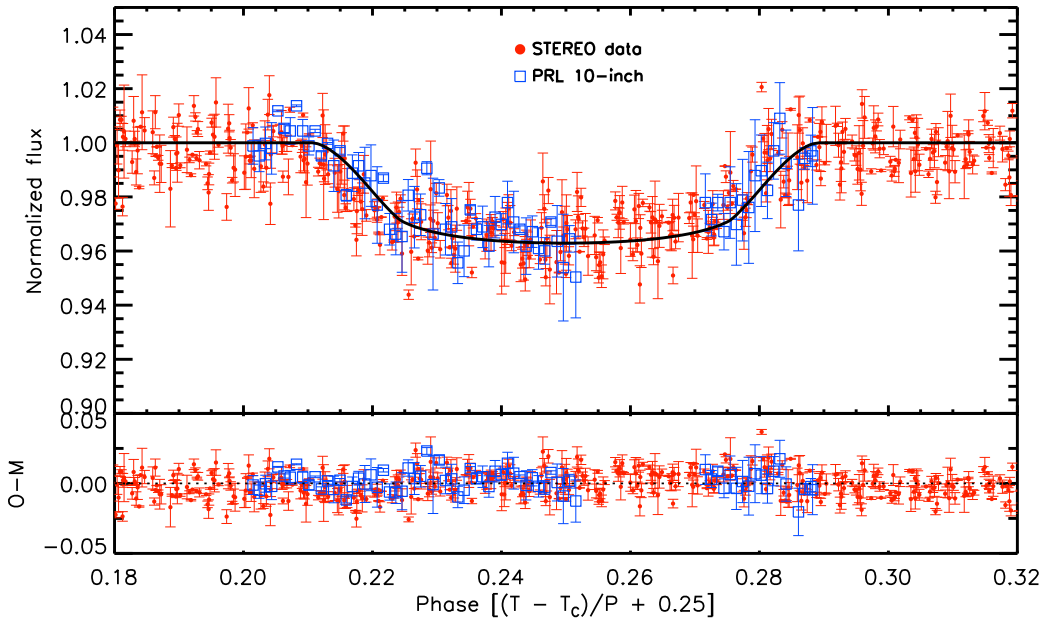

Figure 3. Top panel: transit curve obtained from *STEREO* data and PRL 10-inch telescope is plotted based on the parameters from EXOFAST. The *STEREO* data are plotted with (red) filled circles and the PRL 10-inch telescope data are plotted with open (blue) squares along with their individual error bars. (Colours are only in online version.) Bottom panel: observed-fit residuals are plotted. For better visual representation, the *x*-axis in phase is shifted by 0.25 so that the central primary transit crossing point (T_c) occurs at phase 0.25 instead of 0.

errors). Based on the transit depth of $0.0317^{+0.0013}_{-0.0012}$ mag, the radius of the secondary is estimated to be $R_B = 0.344^{+0.0097}_{-0.01}$ $R_\odot$ with an accuracy of ∼5–6 per cent (formal errors). The radius estimated here is in good agreement with the value given by Wraight et al. (2012).

Metallicity and the iron abundance of the system are accurately determined in this work as -0.105 ± 0.03 and -0.025 ± 0.05 (see Table 3) by spectroscopic analysis. From the models for M dwarfs (Baraffe et al. 1998), we estimate the $T_{\rm eff}$ of the secondary star for a mass of ∼0.3 $M_\odot$ (from this work) and an age of ∼2 Gyr (Casagrande et al. 2011), as 3437 K for a [M/H] of 0.0, and 3643 K for a [M/H] of −0.5. From Baraffe et al. (1998) models, the radius for 0.3 $M_\odot$ turns out to be 0.29 $R_\odot$ for [M/H] = 0.0 and 0.28 $R_\odot$ for [M/H] = −0.5. Clearly, these theoretically derived radius values are lower than the observations presented here.

The binary system has an inclination angle of $84.^\circ9^{+0.61}_{-0.5}$. The rotational velocity of the primary star obtained by SME analysis, as mentioned in Table 3, is 40 km s^{-1}, which matches when measured by the width of the cross-correlation function. This value is comparatively lower than the reported rotational velocities for similar

F-type stars (Gĺębocki & Gnaciński 2005). With the knowledge of rotational velocity of the primary star and its radius of $\sim$2.03 $R_\odot$ from Table 1, the projected spin period $P/\sin i$ of the primary star is calculated to be 2.422 d, which is close to the observed orbital period of the system. The eccentricity of the system, calculated as 0.0198, makes it close to circular. Since the orbital and rotational periods for the star are synchronous, this star forms another evidence for tidal circularization playing role in a close binary system (Mazeh 2008).

The detailed spectral analysis of the high S/N HET spectra gives us $T_{\rm eff}$= 6752 $\pm$ 52 K, [Fe/H] = $-$0.025 $\pm$ 0.05 for $\log g$ = 3.96 $\pm$ 0.1. The temperature indicates an F-type primary star. It may be mentioned that Masana et al. (2006) obtained a $T_{\rm eff}$ of 6936 $\pm$ 70 K based on *V* and Two Micron All Sky Survey (2MASS) *JHK* photometry, while Casagrande et al. (2011) reported a value of 6837 $\pm$ 80 K based on improved colour calibration of the same bands. Our results are more reliable as they are based on detailed spectral analysis from high S/N spectra. Furthermore, these results are substantiated by the fact that the RV and photometry data are not able to constrain a solution in EXOFAST by using the previously cited $T_{\rm eff}$ value of 6936 $\pm$ 70 K. Using $T_{\rm eff}$, [Fe/H] and $\log g$ derived from this work, the mass and radius of the primary star obtained from mass–radius relationship (Torres et al. 2010) are 1.48 $M_\odot$ and 2.11 $R_\odot$, respectively, consistent with the values reported in literature (see Table 1).

Future spectroscopic observations of this star during transit will enable us to observe the Rossiter–McLaughlin effect (Scott Gaudi & Winn 2007), and help determine whether the secondary star is in retrograde or prograde orbital motion with respect to the rotation of the primary. This may lead to a better understanding of the binary formation mechanisms at a primordial stage. Future high-resolution near-infrared observations will be able to provide dynamical masses of the system.

ACKNOWLEDGEMENTS

This work has been made possible by the PRL research grant for PC and the PRL–DOS (Department of Space, Government of India) grant for the PARAS spectrograph. This work was partially supported by funding from the Center for Exoplanets and Habitable Worlds. The Center for Exoplanets and Habitable Worlds is supported by the Pennsylvania State University, the Eberly College of Science and the Pennsylvania Space Grant Consortium. We thank the observatory staff at the Hobby–Eberly Telescope (HET) and the PRL Mt Abu telescope from where the data were obtained. HET is a joint project of the University of Texas at Austin, the Pennsylvania State University, Stanford University, Ludwig-Maximilians-Universität München and Georg-August-Universität Göttingen. The HET is named in honour of its principal benefactors, William P. Hobby and Robert E. Eberly. PC acknowledges help from Varun Dongre and Vishal Shah for their technical support during the course of data acquisition. We thank the UKSSDC team for the STEREO archival data. This research has made use of the ADS and CDS data bases, operated at the CDS, Strasbourg, France. We also thank the referee, Barry Smalley, for detailed and insightful comments which have helped to improve the quality of the paper significantly.

REFERENCES

Ammler-von Eiff M., Reiners A., 2012, A&A, 542, A116
Andersen J., 1991, A&AR, 3, 91
Baraffe I., Chabrier G., 1996, ApJ, 461, L51
Baraffe I., Chabrier G., Allard F., Hauschildt P. H., 1998, A&A, 337, 403
Beatty T. G. et al., 2007, ApJ, 663, 573
Bender C. F. et al., 2012, ApJ, 751, L31
Berger D. H. et al., 2006, ApJ, 644, 475
Bouchy F., Pepe F., Queloz D., 2001, A&A, 374, 733
Bouchy F., Pont F., Melo C., Santos N. C., Mayor M., Queloz M., Udry S., 2005, A&A, 431, 1105
Bouchy F. et al., 2011a, A&A, 525, A68
Bouchy F. et al., 2011b, A&A, 533, A83
Casagrande L., Shönrich R., Asplund M., Cassini S., Ramírez I., Meléndez J., Bensby T., Feltzing S., 2011, A&A, 530, 138
Chakraborty A. et al., 2014, PASP, 126, 133
Eastman J., Gaudi B. S., Agol E., 2013, PASP, 125, 83
Edvardsson B., Andersen J., Gustafsson B., Lambert D. L., Nissen P. E., Tomkin J., 1993, A&A, 275, 101
Fernandez J. M. et al., 2009, ApJ, 701, 764
Gĺębocki R., Gnaciński P., 2005, in Favata F., Hussain G. A. J., Battrick B., eds, Proceedings of the 13th Cambridge Workshop on Cool Stars, Stellar Systems and the Sun, ESA SP-560. ESA, Noordwijk, p. 571
Gómez Y. et al., 2013, ApJ, 768, 79
Gray R. O., 2009, Documentation for SPECTRUM v2.76, Appalachian State University
Hatzes A. P., Cochran W. D., 1992, in Ulrich M. H., ed., ESO Workshop on High Resolution Spectroscopy with the VLT. European Southern Observatory, Garching bei Munchen, Germany, p. 275
Huber D. et al., 2013, ApJ, 767, 127
Johnson J. A. et al., 2011, AJ, 141, 16
López-Morales M., 2007, ApJ, 660, 732
López-Morales M., Ribas I., 2005, ApJ, 631, 1120
Masana E., Jordi C., Ribas I., 2006, A&A, 450, 735
Mazeh T., 2008, in Goupil M. J., Zahn J. P., eds, EAS Publ. Ser. Vol. 29, Tidal Effects in Stars, Planets and Disks. EDP Sciences, France, p. 1
Mullan D. J., MacDonald J., 2001, ApJ, 559, 353
Nordström B., Stefanik R. P., Latham D. W., Andersen J., 1997, A&AS, 126, 21
Nordström B. et al., 2004, A&A, 418, 989
Piskunov N., Valenti J., 2002, A&A, 385, 1095
Pont F., Melo C. H. F., Udry S., Queloz D., Mayor M., Santos N. C., 2005a, A&A, 433, L21
Pont F., Bouchy F., Melo C., Santos N. C., Mayor M., Queloz D., Udry S., 2005b, A&A, 438, 1123
Pont F. et al., 2006, A&A, 447, 1035
Ramsey L. W. et al., 1998, Proc. SPIE, 3352, 34
Sangaralingam V., Steven I., 2011, MNRAS, 418, 1325
Scott Gaudi B., Winn J. N., 2007, ApJ, 655, 550
Stempels H., Collier Cameron A., Hebb L., Smalley B., 2007, MNRAS, 379, 773
Torres G., Andersen J., Giménez A., 2010, A&AR, 18, 67
Torres G., Fischer D. A., Sozzetti A., Buchhave L., Winn Joshua N., Holman Matthew J., Carter Joshua A., 2012, ApJ, 757, 161
Tull R., 1998, Proc. SPIE, 3355, 21
Valenti J. A., Fischer D. A., 2005, ApJS, 159, 141
Valenti J. A., Piskunov N., 1996, ApJS, 118, 595
Wang S. X. et al., 2012, ApJ, 761, 46
Whittaker G. N., Stevens I. R., Sangaralingam V., 2013, MNRAS, 431, 3456
Wraight K. T., White G. J., Bewsher D., Norton A. J., 2011, MNRAS, 416, 2477
Wraight K. T., Fossati L., White G. J., Norton A. J., Bewsher D., 2012, MNRAS, 427, 2298
Zucker S., 2003, MNRAS, 342, 1291

This paper has been typeset from a TEX/LATEX file prepared by the author.